NANO LETTERS

pubs.acs.org/NanoLett

Letter

Multicomponent Copolymer Planar Membranes with Nanoscale Domain Separation

Maryame Bina, Agata Krywko-Cendrowska, Davy Daubian, Wolfgang Meier, and Cornelia G. Palivan*

Cite This: *Nano Lett.* 2022, 22, 5077−5085

Read Online

ACCESS | Metrics & More | Article Recommendations | Supporting Information

ABSTRACT: Domain separation is crucial for proper cellular function and numerous biomedical technologies, especially artificial cells. While phase separation in hybrid membranes containing lipids and copolymers is well-known, the membranes' overall stability, limited by the lipid part, is hindering the technological applications. Here, we introduce a fully synthetic planar membrane undergoing phase separation into domains embedded within a continuous phase. The mono- and bilayer membranes are composed of two amphiphilic diblock copolymers (PEO_{45}-*b*-$PEHOx_{20}$ and $PMOXA_{10}$-*b*-$PDMS_{25}$) with distinct properties and mixed at various concentrations. The molar ratio of the copolymers in the mixture and the nature of the solid support were the key parameters inducing nanoscale phase separation of the planar membranes. The size of the domains and resulting morphology of the nanopatterned surfaces were tailored by adjusting the molar ratios of the copolymers and transfer conditions. Our approach opens new avenues for the development of biomimetic planar membranes with a nanoscale texture.

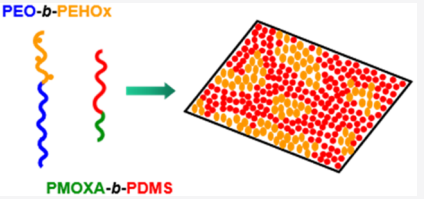

KEYWORDS: *Self-assembled membranes, biomimicry, amphiphilic block copolymers, phase separation, domain formation, surface functionalization*

Nature is an unlimited source of inspiration when it comes to the fabrication of functional nanomaterials. In particular, textured surfaces represent an interesting example of naturally occurring architectures. The cellular membrane itself can be considered as a textured surface, yet dynamic and in constant interaction with its environment. The presence of cholesterol-rich lipid domains or rafts of higher rigidity on the membrane surface leads to a particular membrane composition that regulates the presence of specific proteins.[1,2] In a biomimicry approach, lipid vesicles were used as models for cell membranes,[3] before block copolymers started to be incorporated, which led to the formation of hybrid nanostructures with a patterned surface morphology.[4−6] Polymers are compounds of choice for the fabrication of biomimetic textured surfaces due to their varied chemical and mechanical properties. Polymer-based patterned surfaces can be obtained using material ablation, for example, laser patterning[7] and plasma etching,[8] or microfabrication techniques, such as photolithography[9] and nanoimprint lithography.[10] However, these techniques require advanced machinery and the use of hazardous chemicals[11] or procedures such as UV irradiation[12] for surface modification while not allowing a liquid mosaic structure of the films to be obtained.[7−10,13,14] Also, the roughness of such patterned surfaces affects the adhesion of fibroblasts[13] and neuronal cells.[14] Therefore, they are unsuitable for the fabrication of biomimetic planar membranes on solid supports. Another method to obtain patterned surfaces is grafting polymer brushes onto solid supports composed of one[15,16] or mixed[17−20] homopolymers. Mechanical patterning of polymer brushes is achieved by lithography deposition of distinct functional groups on the same surface, such as amino and carboxylic acid terminal groups[21] or nitro and amino groups.[22] Steric hindrance causes polymer brushes to be less compact than planar films achieved by mechanically assisted polymer assembly, such as Langmuir−Blodgett and Langmuir−Schaefer methods,[23,24] and might prevent them from biomimicry applications. On the contrary, the latter methods allow a control of the membrane density, by adjusting the pressure at which the transfer is performed. Additionally, hybrid membranes composed of lipids and amphiphilic diblock copolymers were already reported to undergo phase separation.[25−28] However, such hybrid membranes have limited mechanical stability due to the lipid domains, which restricts their range of applications. While several studies point at phase separation in the membrane of a hybrid lipid-polymer,[29−31] multicomponent synthetic vesicles,[32,33] or annealed polymer films[34] and their mixtures casted on solid supports,[35,36] phase separation of dual-component synthetic planar membranes has not yet been reported. The assembly of multiple copolymer species onto a solid support is expected to affect their behavior, whereas the morphology and properties of the support constitute additional

Received: January 25, 2022
Revised: June 7, 2022
Published: June 30, 2022

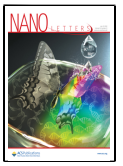

https://doi.org/10.1021/acs.nanolett.2c00332
Nano Lett. 2022, 22, 5077−5085

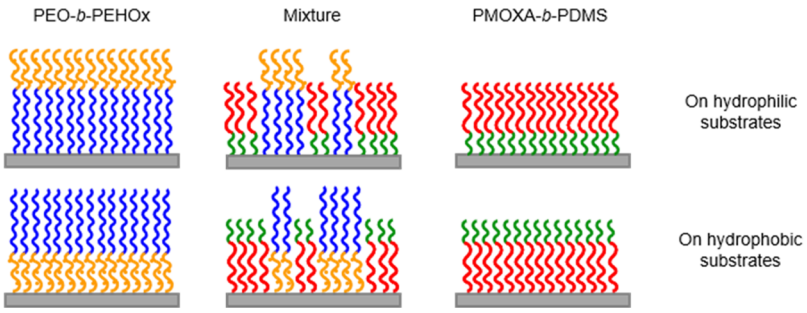

Figure 1. Scheme of the PEO-*b*-PEHOx and PMOXA-*b*-PDMS copolymers adopting a specific orientation depending on the substrate nature. Side chains are present on the PEHOx block to illustrate steric hindrance.

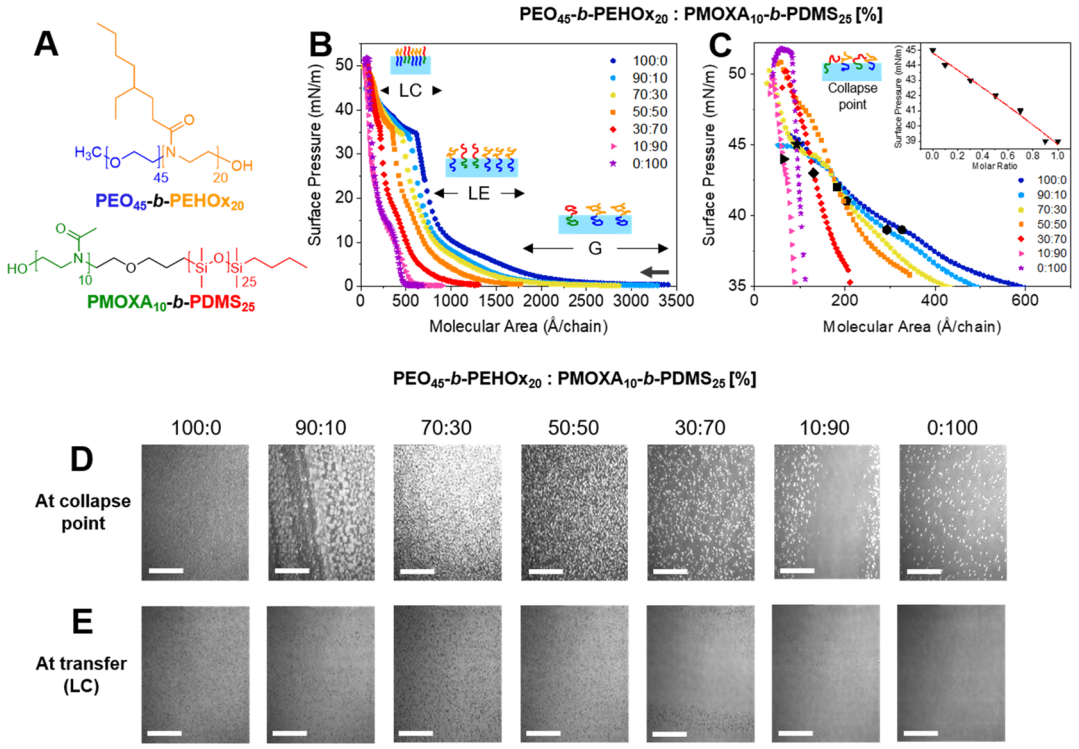

Figure 2. (A) Chemical structures of PEO_{45}-*b*-$PEHOx_{20}$ and $PMOXA_{10}$-*b*-$PDMS_{25}$: hydrophilic blocks (blue and green) and hydrophobic blocks (orange and red). (B) Surface pressure−molecular area isotherms of mixed PEO_{45}-*b*-$PEHOx_{20}$ and $PMOXA_{10}$-*b*-$PDMS_{25}$ at 100:0; 90:10; 70:30; 50:50; 30:70; 10:90; and 0:100 molar ratios. The values indicate the corresponding molar fraction of PEO_{45}-*b*-$PEHOx_{20}$ in relation to $PMOXA_{10}$-*b*-$PDMS_{25}$, and the arrow indicates the compression direction. (C) Zoom-in of the LC phase showing the curve shapes toward the monolayers' breaking points with an inset image representing the trend of the chosen surface pressure values for the LB and LS transfers. (D) Brewster angle micrographs (BAMs) of PEO_{45}-*b*-$PEHOx_{20}$:$PMOXA_{10}$-*b*-$PDMS_{25}$ monolayer mixtures at 100:0; 90:10; 70:30; 50:50; 30:70; 10:90; and 0:100 molar ratios at the air/water interface at the breaking point and (E) local structure at transfer. The first number indicates the composition of the mixture. The scale bar corresponds to 100 μm. The isotherms were registered at least three times for each mixture composition.

parameters influencing a range of surface properties, such as texturization,[17] roughness,[37] wettability,[38] differential cell affinity,[39] or antibiofouling properties.[40] While multicomponent polymer membranes are expected to provide more stable and robust platforms compared to the lipid counterpart for study of various processes and interactions with biomolecules, drugs, or synthetic catalysts, to the best of our knowledge, such synthetic membranes are not yet reported. Here, we introduce surfaces with a nanoscale texture that are based on soft membranes obtained by the self-assembly of two different amphiphilic copolymers onto a solid support (Figure 1). We aim to achieve the nanotexture of the planar membranes by inducing a phase separation of the dissimilar copolymers. While phase separation has been obtained by annealing of films formed by spin-coating of a copolymer,[34−36] that approach is incompatible with biological applications and would lead to a loss of the order induced by self-assembly. Conversely, we induce phase separation by a completely different approach, the self-assembly of a mixture of two amphiphilic copolymers with different molecular properties in specific ratios that are assembled at the air/water interface. We chose poly(ethylene oxide)-*block*-poly(2-(3-ethylheptyl)-2-oxazoline) (PEO−*b*−PEHOx) and poly(2-methyloxazoline)-*block*-poly(dimethylsiloxane) (PMOXA−*b*−PDMS) due to their distinct properties (flexibility, molecular size, and chain length) that allow triggering the resulting morphology of the planar membranes when mixed together. We deposited the membranes using a combination of Langmuir−Blodgett (LB) and Langmuir−Schaeffer (LS) transfers, which allows for the control of the morphology and composition of the membranes

https://doi.org/10.1021/acs.nanolett.2c00332
Nano Lett. 2022, 22, 5077−5085

on a supramolecular level. To investigate the influence of each copolymer type, we deposited mono- and bilayer membranes composed of PMOXA−*b*−PDMS and PEO−*b*−PEHOx, mixed at different molar ratios. A combination of Brewster angle microscopy (BAM), ellipsometry, contact angle (CA) measurements, atomic force microscopy (AFM), and confocal laser scanning microscopy (CLSM) was used to characterize the membranes. In addition, the use of the same substrate with either hydrophilic or hydrophobic surface functionalization served understanding the substrate's role on the resulting morphology of the multicomponent membranes. We were interested to establish how the mixture of amphiphilic copolymers forms domains by phase separation when transferred on a solid support and which is the role of the copolymers (chemical nature, flexibility of the polymer chains, immiscibility) on their self-organization upon controlled compression at the air/water interface. In addition, we explored how the membrane thickness and surface properties depend both on the molar ratio of the diblock copolymers and on the wettability of the solid support. Interestingly, the copolymer with less flexible chains, PEO_{45}−*b*−$PEHOx_{20}$, was the one governing the phase separation, while the other copolymer $PMOXA_{10}$-*b*-$PDMS_{25}$ influenced the domain size.

Such soft nanotextured membranes generated in a biomimicry manner taking inspiration from the domains in cell membranes open new avenues for simultaneous and controlled combination with active compounds (proteins, drugs, catalysts) to engineer multifunctional surfaces with a nanoscale texture.

In order to obtain planar membranes composed of two different amphiphilic copolymers, we used mixtures of PEO_{45}-*b*-$PEHOx_{20}$ (referred to as PEO−PEHOx) and $PMOXA_{10}$-*b*-$PDMS_{25}$ (referred to as PMOXA−PDMS) at molar ratios from 0 to 1 for both components (Figure 2A). For simplicity, molar ratios are given using percentage ratios, e.g., 30:70, where the first value refers to PEO−PEHOx molar content and the second one refers to PMOXA−PDMS molar content.

In the first stage, we formed monolayers at the air/water interface. Langmuir isotherms for PEO−PEHOx, PMOXA−PDMS, and their mixtures recorded during the formation of the monolayers display phase transitions. These reflect the changes in the spatial organization of the amphiphilic species, evident from changes in the curve shape (Figure 2B). For the PEO−PEHOx diblock, two clear transitions are observed: a minor one below 10 mN m^{-1} represents the monolayer shift from the gaseous phase (G) to the liquid expanded (LE) phase, followed by a second, stronger transition around 35 mN m^{-1} (Figure 2B). Because of the slow increase in surface pressure in that area, this latter transition represents the coexisting LE and liquid condensed (LC) phases of the PEO−PEHOx chains.[41,42] Upon compression, copolymer mixtures undergo such transitions from the G phase, where copolymer chains are widely separated, to the LE phase and further to the LC phase, where the chains occupy a small surface area.[43] By contrast, for the PMOXA−PDMS copolymer, only one transition around 12 mN m^{-1} is clearly visible, followed by a rapid escalation in surface pressure to an LC phase. This difference in behavior is caused by the flexibility and linear geometry of the PMOXA−PDMS copolymer as compared to PEO−PEHOx.[44] Large differences in flexibility and initial area occupancy expressed in Å/chain at the same pressure value, i.e., 3000 Å/chain for PEO−PEHOx and 500 Å/chain for PMOXA−PDMS, combined with the characteristic shape of their isotherms, indicate their distinct conformations at the air/water interface. This difference originates both from the hydrophobic side chain on the PEHOx and the plasticity of the PDMS block.[45,46] Binary mixtures of these copolymers would therefore theoretically undergo phase or at least domain separation at the microscopic level. When these block copolymers were mixed, we observed the characteristic transitions of both copolymers at pressure values comparable to those observed for the pure phases, which indicates their independent behavior and supports the occurrence of phase separation. Additionally, the plateau corresponding to the PEO−PEHOx transition from the LE to LC phase at 35 mN m^{-1} shifted toward lower mean molecular area values with increasing proportions of PMOXA−PDMS in the mixture. Noticeably, due to the side chain of PEHOx, PEO−PEHOx occupied a larger molecular area as compared to PMOXA−PDMS resulting in lower pressure at the monolayer collapse point, i.e., 51 mN m^{-1} for PMOXA−PDMS versus 45 mN m^{-1} for PEO−PEHOx. The collapse pressure (named also breaking pressure) refers to the maximum surface pressure reachable for a monolayer before its rupture. PMOXA−PDMS was expected to adopt a straight conformation in the LC phase because of its high compressibility[47] while forming domains of densely packed chains (Figure 2B). On the contrary, PEO−PEHOx formed soft regions with its chains occupying relatively more space. Mixed monolayers were compressible up to 50 mN m^{-1} where they suddenly ruptured for all molar ratios with the exception of the 90:10 mixture and PEO−PEHOx alone (Figure 2C). A plateau was observed indicating that the bulky PEHOx side chain contributed to bringing resistance to compression.[48]

The recording of Langmuir compression isotherms is a necessary step before the transfer of the films, because assessing the stability of the monolayer at the air/water interface is a prerequisite for its effective transfer onto a solid support.[49] To obtain densely packed and homogeneous membranes, deposition in the LC phase for each binary mixture is preferred.[44] Based on the registered breaking point values of the Langmuir isotherms (Table S2), the surface pressures suitable for transfer would correspond to ∼85% of the surface pressure at the collapse point. At this pressure level, the isotherm slopes are steep but below the breaking point, thus ensuring that the molecules are in a continuous condensed layer at the interface. With increasing contents of PMOXA−PDMS, higher surface pressures for deposition were reached, due to higher compressibility of the PDMS chains (Figure 2A). During the compression of the monolayers, BAM allowed for the observation of the morphology changes. After letting the copolymer chains adopt their most favorable orientation during the initial equilibration period, the monolayer was compressed toward the breaking point. Copolymer mixtures became more densely packed, and bright circular surface micelles were observed on top of the underlying homogeneous monolayer (Figure 2D). Such structures demonstrate the multiphasic nature of the monolayer at the air/water interface.[50,51] For the 90:10 mixture, with the maximum surface pressure at ∼45 mN m^{-1}, the presence of bright and dark regions at the breaking point indicates a phase segregation of the copolymer species according to their chemical affinity. For mixtures containing more closely matching concentrations of PEO−PEHOx and PMOXA−PDMS (70:30, 50:50, and 30:70), a continuous layer of micelles appeared, the number of which increased with

https://doi.org/10.1021/acs.nanolett.2c00332
Nano Lett. 2022, 22, 5077−5085

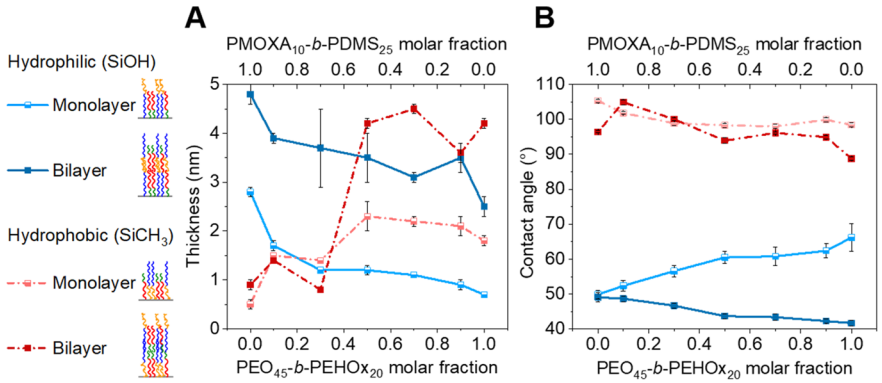

Figure 3. (A) Thickness dependence of the polymer membranes with PEO_{45}-*b*-$PEHOx_{20}$ and $PMOXA_{10}$-*b*-$PDMS_{25}$ molar fractions for the investigated samples. (B) Contact angle dependence of polymer membranes with PEO_{45}-*b*-$PEHOx_{20}$ and $PMOXA_{10}$-*b*-$PDMS_{25}$ molar fractions, measured with water as the probe liquid. For each point, the measurements were performed at least three times for three different membranes.

PEO−PEHOx content (Figure 2D). Additionally, for mixtures where PEO−PEHOx constituted the predominant compound (90:10) and for PEO−PEHOx alone, dark round micelles appeared (Figure 2E). In opposition to what has been observed for hybrid monolayers composed of lipids and polymers,[27] no obvious phase separation occurred at the air/water interface for the present block copolymer-only mixtures. However, differential scanning calorimetric measurements of the mixtures showed the immiscibility behavior of the copolymers. The glass transition temperature (T_g) of PDMS in the area of −120 °C (Figure S1) gradually becomes invisible with increasing amounts of PEO−PEHOx, as the melting peaks of PEO and PEHOx appear around 50 °C. When the content of PEO−PEHOx increases, the glass transitions of PEO at −40 °C and PEHOx at 10 °C become more and more apparent,[52,53] demonstrating a clear phase separation with the T_g values corresponding to those of the individual homopolymers (e.g., 50:50 mixture). This behavior emphasizes the difference in flexibility of both domains, with PMOXA−PDMS chains being more flexible than those of PEO−PEHOx.

In the next step, we prepared suitable solid substrates for the transfer of the films by selecting Si wafers, as they are well-characterized in terms of surface properties,[54] nontoxic, and easily rendered hydrophilic or hydrophobic.

Hydrophilic functionalization of Si surfaces was achieved by solvent and subsequent UV ozone cleaning to remove any remaining organic residues from the surface while generating −OH surface groups (Figure S2). While LB and LS techniques are powerful tools to fabricate biomimetic films of controlled grafting density, the transfer itself is a complex process, during which amphiphilic molecules can rearrange to achieve their most favorable thermodynamic minimum.[55] The functionalization of the substrate directed the hydrophilic blocks of the copolymers toward the surface while leaving their hydrophobic counterparts facing up. The second layer was deposited using hydrophobic interactions between the blocks on top of the monolayer and the hydrophobic blocks facing upward at the air/water interface using the horizontal LS transfer.

We calculated the transfer ratio (TR) as the ratio between area diminution (Δ) of the trough during the transfer and the surface area of the solid support to establish the efficiency of the Langmuir monolayer transfer onto a solid support (eq S1).[56] TR values were close to unity for each mixture of copolymers studied, indicating defect-free films and complete coverage of the hydrophilic silicon substrate (Table S1). TR values close to unity can also imply a morphologically inhomogeneous deposition where parts of the solid substrate are covered with a monolayer, no layer, and/or multiple layers in other areas.[55] However, the rigidity of the block copolymers, in addition to the presence of the side chain of the PEHOx, prevents such deposition scenarios, which are typically observed for lipid monolayers that adopt a more favorable conformation through flip-flop mechanisms.[57] Here, the copolymers remained in a straight conformation from their compression at the air/water interface up until their transfer onto the substrate, as indicated by their TR values. This ensured full substrate coverage and that the spatial orientation of the polymers is maintained throughout the transfer.

Deposition of the monolayers onto hydrophobic substrates proceeded via a reverse procedure as compared to the hydrophilic surface. Using the horizontal LS step, the monolayers attach via hydrophobic blocks to the silanized Si surface. Successive LB transfer with a downward motion followed by an upward motion was found to provide the highest quality in terms of bilayer film coverage. Calculated TR values of the monolayers formed at the air/water interface and transferred onto hydrophobic substrates were close to unity for all mixtures except for the pure PMOXA−PDMS diblock, for which the TR was 0.18. Such a low TR value indicates very low coverage of the substrate and inefficient transfer or a different orientation of the diblock chains at the air/water interface. Considering the compressibility of PMOXA−PDMS (Figure 2), the surface pressure value below the breaking point of its Langmuir monolayer presumably hindered the formation of a layer dense enough to obtain the necessary straight conformation of the polymer chains. Unlike for the bilayers obtained on hydrophilic supports, TR values for bilayers deposited on hydrophobic supports varied significantly with the content of PMOXA−PDMS. While the deposition of a bilayer composed solely of PMOXA−PDMS was not successful (TR equal to 0), after even slight addition of PEO−PEHOx (10:90), the TR value increased to ∼0.6 and stayed on a comparable level with increasing amounts of PEO−PEHOx, with a sudden decrease for the 70:30 mixture to ∼0.4. A TR value close to unity was calculated for solutions containing a majority of PEO−PEHOx (90:10 and PEO−PEHOx alone), meaning that PEO−PEHOx contributed to the stability and substrate coverage of the bilayers. Together with the domain separation visible in BAM micrographs (Figure 2D), this indicates the influence of this copolymer on the

https://doi.org/10.1021/acs.nanolett.2c00332
Nano Lett. 2022, 22, 5077−5085

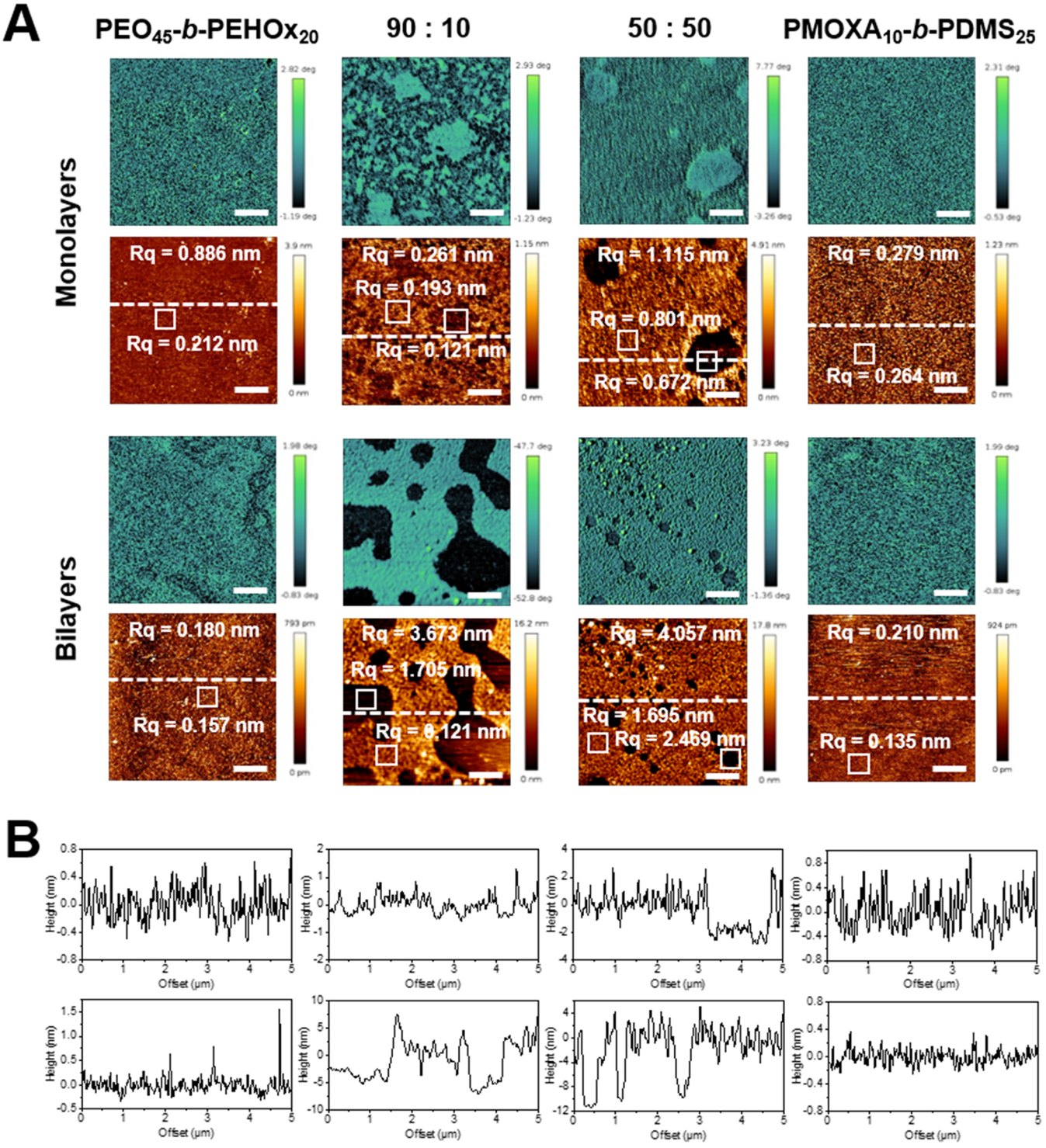

Figure 4. (A) Shift in phase (upper row, blue cyan) and height type (lower row, red orange) images of one-component films of PEO_{45}-*b*-$PEHOx_{20}$ and $PMOXA_{10}$-*b*-$PDMS_{25}$ and of 90:10 and 50:50 mixture films transferred onto hydrophilic silicon wafers in the forms of monolayers and bilayers. Imaged in water. Scale bar 1 μm. (B) Height profiles of the corresponding copolymer biomimetic membranes displaying height (nm) vs offset (μm). AFM measurements were performed for each membrane in five different regions and for at least three samples of the same composition.

transfer and the morphology of the second layer. Since bare Si wafers exhibit a uniform surface on an atomic level,[58] the copolymer layers attached to the surface with no significant influence from the morphology of the substrate, resulting in TR values close to unity. Contarily, a morphological effect for the TR values of the second layer depended on the molar ratio of both diblocks and prompted a morphologic effect of the first layer as well.

The evolution of the thickness as measured by ellipsometry depended on the molar ratio of both components (Table S3). Increasing amounts of the PEO−PEHOx led to thinner films on hydrophilic surfaces (Figure 3A). The thickness of the $PMOXA_{10}$-$PDMS_{25}$ monolayer of 2.8 ± 0.1 nm was in good

https://doi.org/10.1021/acs.nanolett.2c00332
Nano Lett. 2022, 22, 5077−5085

agreement with reported data, being between 1.8 nm for $PMOXA_9$-*b*-$PDMS_{16}$[44] and 4.5 nm for $PMOXA_9$-*b*-$PDMS_{37}$.[59] The decrease in thickness with an increasing proportion of PEO−PEHOx is due to the weak hydrophobicity of the PEHOx blocks that contain 33% of hydrophilic volume fraction[53] as well as the short length of the PEHOx block, which could lead to the shrinkage of the copolymer. On the other hand, monolayers deposited onto hydrophobic substrates followed an opposite trend, where the thickness was ∼0.5 nm for PMOXA−PDMS alone and increased with PEO−PEHOx content up to ∼2 nm. These values are however not reflecting the actual layer thicknesses and should be interpreted as a function of the surface coverage. The low thickness of PMOXA−PDMS films is associated with low TR, indicating poor adhesion of the copolymer chains to the hydrophobic substrate (Table S3, TR = 18%), possibly due to the chemical inhomogeneity of the silanized silicon substrate (Figure S5). PMOXA−PDMS chains form thin disorganized layers to which the second layer cannot attach (Table S3, TR = 0%). Based on the calculated TR values (Tables S2 and S3), mono- and bilayers were obtained with molar ratios ranging from 90 to 100% and from ∼50 to 100%, respectively. This shows the rigidifying effect of PEO−PEHOx on the overall membrane structure leading to actual dense layers.

To determine the membrane orientation after monolayer and bilayer transfers, their CAs were measured using water as the probe liquid (Figure 3B). When deposited on a hydrophilic surface, hydrophobic blocks in the monolayer face upward, which results in higher CA values than for the bilayers. With increasing content of PEO−PEHOx in the monolayer, the CA value increased from 50 to 65° and the surface became more hydrophobic, which indicates a higher hydrophobicity strength of PEHOx when compared to the PDMS block. An opposite trend was observed for bilayers, resulting in CA decreasing from 50 to 40° when films contain more PEO−PEHOx, which indicates that the PEO block is more hydrophilic than the PMOXA block. CA values for mono- and bilayers deposited on hydrophobic substrates were close to those reported for the silanized silicon wafer, i.e., 104°.[60] Based on the low TR values (Table S2), these results indicate that either the water droplet interacted with the surface of the substrate through the polymer layers or there was an incomplete coverage for membranes where the major component was PEO−PEHOx. On the contrary, bilayers containing a majority of PMOXA−PDMS (90 to 100%) offered full substrate coverage in agreement with the calculated TR parameter and hydrophilic CA values.

To assess the stability of the films in air, AFM of the corresponding membrane deposited on hydrophilic and hydrophobic solid substrates was measured (Figures S3 and S6). They exhibited carpet-like morphologies covered with round nanostructures, eclipsing the details of the domain separation. However, this nonuniform morphology and these round nanoassemblies formed while drying can be related to the domain formation in the membranes after the transfer.

To gain insight into the morphology of the membranes and relate it to the TR values, thickness and wettability of the obtained mono- and bilayers deposited onto hydrophilic Si, we measured the membranes using AFM in water (Figure 4). While BAM served only to observe the monolayer at the air water interface on a macroscale, we used the advantage of high resolution in AFM to uncover the subtle differences in morphology between the membranes. Membranes composed only of one diblock copolymer exhibited a uniform morphology and low root-mean-square roughness (R_q) ranging between ∼0.1 and 0.3 nm (Figure 4A). The mono- and bilayers transferred onto the hydrophilic Si surface presented uniform and densely packed structures, corresponding well with TR values of one-component membranes. By contrast, membranes obtained from mixtures of copolymers displayed nonuniform morphologies and separated into domains depending on the molar ratio of the respective diblock copolymers. At a 90:10 ratio, monolayers were flat with (R_q = 2.9 nm), exhibiting discontinuous and irregularly shaped niches lower by up to 1 nm in height from the level of the continuous phase (Figure 4A, monolayers). At equal concentrations of both components (50:50), the films had an R_q of 0.7 nm with domains forming isolated islands, suggesting mixed diblock composition within the islands. Bilayers of the same composition (Figure 4A, bilayers) showed height disparities with increasing PEO−PEHOx content leading to the formation of larger flat domains of up to 3 μm in size and an R_q of ∼1.7 nm. Comparing the thicknesses of PMOXA−PDMS mono- and bilayers (2.8 and 4.8 nm, respectively) to the thickness of PEO−PEHOx mono- and bilayers (0.7 and 2.5 nm, respectively) formed on hydrophilic substrates, the difference in height of bilayers corresponds to that of a PMOXA−PDMS monolayer. This indicates that the continuous phase was composed of PMOXA−PDMS. A relatively high R_q value of 1.7 nm within the flatter areas in addition to the difference in their thickness compared to the continuous phase point to a binary composition within the domains as well.

In order explore the domain separation, we used CLSM on bilayers of one-component films and on two-components ones (90:10 and 50:50) at a similar scale as in AFM images (Figure S8). PMOXA−PDMS labeled with a dye allowed us to observe its localization at the surface. The fluorescence intensity increased homogeneously with higher amounts of PMOXA−PDMS in a one-component membrane. Note that the green shades for the PMOXA−PDMS bilayer can be attributed to the film roughness. The domain separation appears for bilayers obtained from mixed copolymers, with black areas corresponding to PEO−PEHOx domains and fluorescent ones associated with PMOXA−PDMS, in agreement with the AFM results. The domain separation of monolayers and bilayers for the 70:30 molar ratio (Figure S4) was evident as in the cases discussed above, while for lower concentrations of PEO−PEHOx (30:70 and 10:90 molar ratios), there was no domain separation. The domain depth for the 70:30 bilayer (Figure S4) was in the range of a few nm, similar to the 90:10 and 50:50 mono- and bilayers (Figure 4). Roughness values calculated for the 70:30, 30:70, and 10:90 ratios were also in the same range, i.e., from 0.63 to 5.7 nm, exhibiting a similar trend for the mono- and bilayer formation according to the changes in the concentration of the respective diblocks. The increase in the R_q of bilayers, compared to monolayers, was more pronounced due to the second layer being deposited onto the first one, the roughness of which was higher than that of the solid support.[61] Additionally, an increase in depth of the domains from ∼1 nm measured for the monolayers to ∼8 nm for the bilayers with the preserved uniform morphology of the continuous phase (R_q = 0.1 nm) has been observed. This additional increase in R_q stems from the diblocks in the second layer attaching to the corresponding diblocks of the first layer due to their chemical affinity indicating higher hydrophobic

https://doi.org/10.1021/acs.nanolett.2c00332
Nano Lett. 2022, 22, 5077−5085

interactions.[62] Hence, it leads to increased disparity in both height and roughness. The shift-in phase AFM images revealed different shift values for the domains and the continuous phase, which followed the same trend as the topographical images. The difference in phase shift was around 10°, which is comparable to the difference observed between lipid and polymer films probed with the same experimental setup.[27] Contrary to the films in air, studied only for their stability, when immersed in water, our synthetic membranes have a comparable behavior to that of lipid-polymer hybrid membranes, their flexibility supporting them as efficient biomimetic membranes. The domains and the continuous phase were chemically uniform and in a stable state but composed of different materials (Figure 4).[63] While a similar aspect can be observed in kinetically trapped structures,[64] they exist in a metastable form, which is completely different to our membranes, where the diblock copolymers are compressed toward each other. The membrane is formed based on physical hindrance and is stabilized by hydrophobic forces before being immobilized onto a solid substrate. It is hereby clear that not only domains formed in water but also that polymer phase separation have been fully reconstituted in an artificial biomimetic solid-supported membrane. Our approach can be utilized for the formation of either different functionalities within one membrane or the insertion of multiple molecules (biomolecules, synthetic compounds, or a combination of thereof) in water.

In this study, we successfully fabricated a nanostructured biomimetic platform based on binary mixtures of amphiphilic block copolymers with different molecular properties. We investigated the complex behavior of binary copolymer mixtures composed of PEO_{45}-*b*-$PEHOx_{20}$ and $PMOXA_{10}$-*b*-$PDMS_{25}$ in terms of their self-assembly into mono- or bilayers, interaction with the solid support, and phase separation of the resulting membranes into domains. Depending on the nature of the substrate and the molar ratio of the copolymers, we observed significant differences in the morphology of the resulting planar membranes. In particular, monolayers and bilayers deposited on a hydrophilic substrate mixed at equal concentrations or with the more rigid copolymer, PEO–PEHOx, as the major component, display an organization on the micro- and nanoscale: the formation of domains surrounded by a continuous phase. The domains are clearly visible and irregularly shaped, thus leading to a patterned polymer surface with texture at nanoscale. Such surfaces with a soft membrane deposited on a solid support represent an essential step forward in obtaining mechanically robust and stable mimics of cellular membranes, as compared to the lipid or lipid-polymer membrane models currently available. In addition, these membranes have flexibility mimicking that of lipid-polymer hybrid membranes, which will favor their combination with active compounds (biomolecules, catalysts, reporting compounds) and specific localization of thereof in separate domains. The control of the nanotexture at the molecular level supports their further development for applications in various areas including multibiosensing, simultaneous catalysis reactions, and optoelectronic device fabrication where the texture gives the material its intrinsic properties.

■ ASSOCIATED CONTENT

Supporting Information

The Supporting Information is available free of charge at https://pubs.acs.org/doi/10.1021/acs.nanolett.2c00332.

Experimental data, materials and methods, protocols for synthesis of PMOXA–PDMS and PEO–PEHOx, surface pressure values corresponding to the respective Langmuir isotherms of polymer solutions, thickness of all films obtained on hydrophobic and hydrophilic substrates measured by ellipsometry, DSC curves of all polymer mixtures, supplementary AFM images in water and in air of mono- and bilayers, and CLSM micrographs of polymer mixtures (PDF)

■ AUTHOR INFORMATION

Corresponding Author

Cornelia G. Palivan − *Department of Chemistry, University of Basel, Basel 4058, Switzerland*; orcid.org/0000-0001-7777-5355; Email: cornelia.palivan@unibas.ch

Authors

Maryame Bina − *Department of Chemistry, University of Basel, Basel 4058, Switzerland*

Agata Krywko-Cendrowska − *Department of Chemistry, University of Basel, Basel 4058, Switzerland*

Davy Daubian − *Department of Chemistry, University of Basel, Basel 4058, Switzerland*

[#]Wolfgang Meier − *Department of Chemistry, University of Basel, Basel 4058, Switzerland*; orcid.org/0000-0002-7551-8272

Complete contact information is available at: https://pubs.acs.org/10.1021/acs.nanolett.2c00332

Author Contributions

Maryame Bina produced the membranes and characterized them by ellipsometry, contact angle, AFM, CLSM, and DSC, while Agata Krywko-Cendrowska supported the interpretation of the results for ellipsometry, contact angle, AFM, and CLSM, and Davy Daubian supported the interpretation of the results for DSC. Wolfgang Meier and Cornelia G. Palivan conceived the original concept and supervised the project. The manuscript was written through contributions of all authors. All authors have given approval to the final version of the manuscript.

Notes

The authors declare no competing financial interest.

[#]Deceased.

■ ACKNOWLEDGMENTS

The authors are grateful for the financial support of this project by the Swiss National Science Foundation (SNSF), the University of Basel, and the National Centre of Competence in Research Molecular Systems Engineering (NCCR-MSE). We gratefully acknowledge Dr. R. Wehr (University of Basel) for providing the PMOXA–PDMS polymer. Dr. S. Di Leone (University of Basel) and Dr. M. Skowicki (University of Basel) are acknowledged for the technical help with experiments and processing the data, Dr. D. Messmer (University of Basel) is acknowledged for fruitful discussions, and Dr. O. Eggenberger (University of Basel) is acknowledged for the final editing of the manuscript.

DEDICATION

We take the opportunity to thank the late Prof. Dr. Wolfgang P. Meier for his strong support and enthusiasm in introducing the concept of this study. He passed away late January of 2022 during the process of this article submission.

REFERENCES

(1) Eggeling, C.; Ringemann, C.; Medda, R.; Schwarzmann, G.; Sandhoff, K.; Polyakova, S.; Belov, V. N.; Hein, B.; Von Middendorff, C.; Schönle, A.; et al. Direct observation of the nanoscale dynamics of membrane lipids in a living cell. *Nature* **2009**, *457* (7233), 1159−1162.

(2) Lenne, P.-F.; Nicolas, A. Physics puzzles on membrane domains posed by cell biology. *Soft Matter* **2009**, *5* (15), 2841−2848.

(3) Elsayed, M. M.; Abdallah, O. Y.; Naggar, V. F.; Khalafallah, N. M. Lipid vesicles for skin delivery of drugs: reviewing three decades of research. *International journal of pharmaceutics* **2007**, *332* (1−2), 1−16.

(4) Hadinoto, K.; Sundaresan, A.; Cheow, W. S. Lipid−polymer hybrid nanoparticles as a new generation therapeutic delivery platform: a review. *Eur. J. Pharm. Biopharm.* **2013**, *85* (3), 427−443.

(5) Discher, D. E.; Ahmed, F. Polymersomes. *Annu. Rev. Biomed. Eng.* **2006**, *8*, 323−341.

(6) LoPresti, C.; Massignani, M.; Fernyhough, C.; Blanazs, A.; Ryan, A. J.; Madsen, J.; Warren, N. J.; Armes, S. P.; Lewis, A. L.; Chirasatitsin, S.; et al. Controlling polymersome surface topology at the nanoscale by membrane confined polymer/polymer phase separation. *ACS Nano* **2011**, *5* (3), 1775−1784.

(7) Singer, J. P.; Kooi, S. E.; Thomas, E. L. Focused laser-induced marangoni dewetting for patterning polymer thin films. *J. Polym. Sci., Part B: Polym. Phys.* **2016**, *54* (2), 225−236.

(8) Agheli, H.; Malmström, J.; Hanarp, P.; Sutherland, D. S. Nanostructured biointerfaces. *Materials Science and Engineering: C* **2006**, *26* (5−7), 911−917.

(9) Prucker, O.; Schimmel, M.; Tovar, G.; Knoll, W.; Rühe, J. Microstructuring of molecularly thin polymer layers by photolithography. *Adv. Mater.* **1998**, *10* (14), 1073−1077.

(10) Hauser, H.; Michl, B.; Schwarzkopf, S.; Kübler, V.; Müller, C.; Hermle, M.; Bläsi, B. Honeycomb texturing of silicon via nanoimprint lithography for solar cell applications. *IEEE Journal of Photovoltaics* **2012**, *2* (2), 114−122.

(11) Yoshino, M.; Matsumura, T.; Umehara, N.; Akagami, Y.; Aravindan, S.; Ohno, T. Engineering surface and development of a new DNA micro array chip. *Wear* **2006**, *260* (3), 274−286.

(12) Mark, D.; Haeberle, S.; Zengerle, R.; Ducree, J.; Vladisavljević, G. T. Manufacture of chitosan microbeads using centrifugally driven flow of gel-forming solutions through a polymeric micronozzle. *J. Colloid Interface Sci.* **2009**, *336* (2), 634−641.

(13) Dalby, M.; Giannaras, D.; Riehle, M.; Gadegaard, N.; Affrossman, S.; Curtis, A. Rapid fibroblast adhesion to 27 nm high polymer demixed nano-topography. *Biomaterials* **2004**, *25* (1), 77−83.

(14) Koufaki, N.; Ranella, A.; Aifantis, K. E.; Barberoglou, M.; Psycharakis, S.; Fotakis, C.; Stratakis, E. Controlling cell adhesion via replication of laser micro/nano-textured surfaces on polymers. *Biofabrication* **2011**, *3* (4), 045004.

(15) Patil, R.; Kiserow, D.; Genzer, J. Creating surface patterns of polymer brushes by degrafting via tetrabutyl ammonium fluoride. *RSC Adv.* **2015**, *5* (105), 86120−86125.

(16) Takahashi, H.; Nakayama, M.; Itoga, K.; Yamato, M.; Okano, T. Micropatterned thermoresponsive polymer brush surfaces for fabricating cell sheets with well-controlled orientational structures. *Biomacromolecules* **2011**, *12* (5), 1414−1418.

(17) Li, M.; Pester, C. W. Mixed polymer brushes for "smart" surfaces. *Polymers* **2020**, *12* (7), 1553.

(18) Martinelli, E.; Agostini, S.; Galli, G.; Chiellini, E.; Glisenti, A.; Pettitt, M. E.; Callow, M. E.; Callow, J. A.; Graf, K.; Bartels, F. W. Nanostructured films of amphiphilic fluorinated block copolymers for fouling release application. *Langmuir* **2008**, *24* (22), 13138−13147.

(19) Motornov, M.; Sheparovych, R.; Katz, E.; Minko, S. Chemical gating with nanostructured responsive polymer brushes: mixed brush versus homopolymer brush. *ACS Nano* **2008**, *2* (1), 41−52.

(20) Zhou, F.; Jiang, L.; Liu, W.; Xue, Q. Fabrication of Chemically Tethered Binary Polymer-Brush Pattern through Two-Step Surface-Initiated Atomic-Transfer Radical Polymerization. *Macromol. Rapid Commun.* **2004**, *25* (23), 1979−1983.

(21) del Campo, A.; Boos, D.; Spiess, H. W.; Jonas, U. Surface Modification with Orthogonal Photosensitive Silanes for Sequential Chemical Lithography and Site-Selective Particle Deposition. *Angew. Chem., Int. Ed.* **2005**, *44* (30), 4707−4712.

(22) Eck, W.; Stadler, V.; Geyer, W.; Zharnikov, M.; Gölzhäuser, A.; Grunze, M. Generation of Surface Amino Groups on Aromatic Self-Assembled Monolayers by Low Energy Electron Beams—A First Step Towards Chemical Lithography. *Adv. Mater.* **2000**, *12* (11), 805−808.

(23) Zhao, B.; Brittain, W. J. Polymer brushes: surface-immobilized macromolecules. *Prog. Polym. Sci.* **2000**, *25* (5), 677−710.

(24) Wu, T.; Efimenko, K.; Genzer, J. Preparing high-density polymer brushes by mechanically assisted polymer assembly. *Macromolecules* **2001**, *34* (4), 684−686.

(25) Kilic, A.; Kok, F. N. Biomimetic lipid bilayers on solid surfaces: models for biological interactions. *Surface Innovations* **2016**, *4* (3), 141−157.

(26) Belegrinou, S.; Menon, S.; Dobrunz, D.; Meier, W. Solid-supported polymeric membranes. *Soft Matter* **2011**, *7* (6), 2202−2210.

(27) Di Leone, S.; Vallapurackal, J.; Yorulmaz Avsar, S.; Kyropolou, M.; Ward, T. R.; Palivan, C. G.; Meier, W. Expanding the Potential of the Solvent-Assisted Method to Create Bio-Interfaces from Amphiphilic Block Copolymers. *Biomacromolecules* **2021**, *22* (7), 3005−3016.

(28) Di Leone, S.; Avsar, S. Y.; Belluati, A.; Wehr, R.; Palivan, C. G.; Meier, W. Polymer−Lipid Hybrid Membranes as a Model Platform to Drive Membrane−Cytochrome c Interaction and Peroxidase-like Activity. *J. Phys. Chem. B* **2020**, *124* (22), 4454−4465.

(29) Dao, T. T.; Brûlet, A.; Fernandes, F.; Er-Rafik, M.; Ferji, K.; Schweins, R.; Chapel, J.-P.; Fedorov, A.; Schmutz, M.; Prieto, M.; et al. Mixing block copolymers with phospholipids at the nanoscale: From hybrid polymer/lipid wormlike micelles to vesicles presenting lipid nanodomains. *Langmuir* **2017**, *33* (7), 1705−1715.

(30) Fauquignon, M.; Ibarboure, E.; Carlotti, S.; Brûlet, A.; Schmutz, M.; Le Meins, J.-F. Large and giant unilamellar vesicle (s) obtained by self-assembly of poly (dimethylsiloxane)-b-poly (ethylene oxide) diblock copolymers, membrane properties and preliminary investigation of their ability to form hybrid polymer/lipid vesicles. *Polymers* **2019**, *11* (12), 2013.

(31) Nam, J.; Beales, P. A.; Vanderlick, T. K. Giant phospholipid/block copolymer hybrid vesicles: Mixing behavior and domain formation. *Langmuir* **2011**, *27* (1), 1−6.

(32) Srinivas, G.; Pitera, J. W. Soft patchy nanoparticles from solution-phase self-assembly of binary diblock copolymers. *Nano Lett.* **2008**, *8* (2), 611−618.

(33) Gera, P.; Salac, D. Three-dimensional multicomponent vesicles: dynamics and influence of material properties. *Soft Matter* **2018**, *14* (37), 7690−7705.

(34) Collin, B.; Chatenay, D.; Coulon, G.; Ausserre, D.; Gallot, Y. Ordering of copolymer thin films as revealed by atomic force microscopy. *Macromolecules* **1992**, *25* (5), 1621−1622.

(35) Polios, I. S.; Soliman, M.; Lee, C.; Gido, S. P.; Schmidt-Rohr, K.; Winter, H. H. Late stages of phase separation in a binary polymer blend studied by rheology, optical and electron microscopy, and solid state NMR. *Macromolecules* **1997**, *30* (15), 4470−4480.

(36) Müller-Buschbaum, P.; Gutmann, J. S.; Stamm, M. Influence of blend composition on phase separation and dewetting of thin polymer blend films. *Macromolecules* **2000**, *33* (13), 4886−4895.

(37) Gu, C.; Meng, X.; Wang, S.; Ding, X. Study on the mutual influence of surface roughness and texture features of rough-textured

https://doi.org/10.1021/acs.nanolett.2c00332
Nano Lett. 2022, 22, 5077−5085

surfaces on the tribological properties. *Proceedings of the Institution of Mechanical Engineers, Part J: Journal of Engineering Tribology* **2021**, *235* (2), 256−273.
(38) Kalaskar, D.; Alshomer, F. Micro-and nanotopographical cues guiding biomaterial host response. *In Situ Tissue Regeneration* **2016**, 137−163.
(39) Lourenço, B. N.; Marchioli, G.; Song, W.; Reis, R. L.; van Blitterswijk, C. A.; Karperien, M.; van Apeldoorn, A.; Mano, J. F. Wettability influences cell behavior on superhydrophobic surfaces with different topographies. *Biointerphases* **2012**, *7* (1), 46.
(40) Maghsoudi, K.; Jafari, R.; Momen, G.; Farzaneh, M. Micro-nanostructured polymer surfaces using injection molding: A review. *Materials today communications* **2017**, *13*, 126−143.
(41) Yu, Z.-W.; Jin, J.; Cao, Y. Characterization of the liquid-expanded to liquid-condensed phase transition of monolayers by means of compressibility. *Langmuir* **2002**, *18* (11), 4530−4531.
(42) Ni, S.; Lee, W.; Li, B.; Esker, A. R. Thermodynamics of the liquid expanded to condensed phase transition of poly (L-lactic acid) in Langmuir monolayers. *Langmuir* **2006**, *22* (8), 3672−3677.
(43) Roberts, G. *Langmuir-Blodgett films*; Springer Science & Business Media: New York, NY, 2013.
(44) Kowal, J.; Wu, D.; Mikhalevich, V.; Palivan, C. G.; Meier, W. Hybrid polymer−lipid films as platforms for directed membrane protein insertion. *Langmuir* **2015**, *31* (17), 4868−4877.
(45) Yang, Y.-L.; Chen, M.-Y.; Tsao, H.-K.; Sheng, Y.-J. Dynamics of bridge−loop transformation in a membrane with mixed monolayer/bilayer structures. *Phys. Chem. Chem. Phys.* **2018**, *20* (9), 6582−6590.
(46) Beales, P. A.; Khan, S.; Muench, S. P.; Jeuken, L. J. Durable vesicles for reconstitution of membrane proteins in biotechnology. *Biochem. Soc. Trans.* **2017**, *45* (1), 15−26.
(47) Shapovalov, V. Langmuir monolayers of polydimethylsiloxane with controllable surface potential. *Thin Solid Films* **1998**, *327*, 816−820.
(48) Rodriguez-Parada, J.; Kaku, M.; Sogah, D. Monolayers and Langmuir-Blodgett films of poly (N-acylethylenimines) with hydrocarbon and fluorocarbon side chains. *Macromolecules* **1994**, *27* (6), 1571−1577.
(49) Oliveira, O. N., Jr Langmuir-Blodgett films-properties and possible applications. *Braz J. Phys.* **1992**, *22* (2), 60−69.
(50) Russell, T. P. Copolymers at surfaces and interfaces. *Curr. Opin. Colloid Interface Sci.* **1996**, *1* (1), 107−115.
(51) Joncheray, T. J.; Bernard, S. A.; Matmour, R.; Lepoittevin, B.; El-Khouri, R. J.; Taton, D.; Gnanou, Y.; Duran, R. S. Polystyrene-b-poly (tert-butyl acrylate) and polystyrene-b-poly (acrylic acid) dendrimer-like copolymers: two-dimensional self-assembly at the air− water interface. *Langmuir* **2007**, *23* (5), 2531−2538.
(52) Zhang, X.-y.; Zhang, P.-y. Polymersomes in nanomedicine-A review. *Current Nanoscience* **2017**, *13* (2), 124−129.
(53) Daubian, D.; Gaitzsch, J.; Meier, W. Synthesis and complex self-assembly of amphiphilic block copolymers with a branched hydrophobic poly (2-oxazoline) into multicompartment micelles, pseudo-vesicles and yolk/shell nanoparticles. *Polym. Chem.* **2020**, *11* (6), 1237−1248.
(54) Stegemann, B.; Gad, K. M.; Balamou, P.; Sixtensson, D.; Vössing, D.; Kasemann, M.; Angermann, H. Ultra-thin silicon oxide layers on crystalline silicon wafers: Comparison of advanced oxidation techniques with respect to chemically abrupt SiO2/Si interfaces with low defect densities. *Appl. Surf. Sci.* **2017**, *395*, 78−85.
(55) Schwartz, D. K. Langmuir-Blodgett film structure. *Surf. Sci. Rep.* **1997**, *27* (7−8), 245−334.
(56) Petty, M. C. *Langmuir-Blodgett Films*; Cambridge University Press: Cambridge, UK, 1996.
(57) Contreras, F.-X.; Sánchez-Magraner, L.; Alonso, A.; Goñi, F. M. Transbilayer (flip-flop) lipid motion and lipid scrambling in membranes. *FEBS letters* **2010**, *584* (9), 1779−1786.
(58) Neergaard Waltenburg, H.; Yates, J. Surface chemistry of silicon. *Chem. Rev.* **1995**, *95* (5), 1589−1673.
(59) Ren, T.; Erbakan, M.; Shen, Y.; Barbieri, E.; Saboe, P.; Feroz, H.; Yan, H.; McCuskey, S.; Hall, J. F.; Schantz, A. B.; et al. Membrane protein insertion into and compatibility with biomimetic membranes. *Advanced Biosystems* **2017**, *1* (7), 1700053.
(60) Wong, J. X.; Yu, H.-Z. Preparation of transparent superhydrophobic glass slides: Demonstration of surface chemistry characteristics. *J. Chem. Educ.* **2013**, *90* (9), 1203−1206.
(61) Rozlosnik, N.; Antal, G.; Pusztai, T.; Faigel, G. Surface roughness in Langmuir-Blodgett multilayer films studied by AFM and X-ray diffraction. *Supramolecular Science* **1997**, *4* (3−4), 215−218.
(62) Yoon, R.-H.; Flinn, D. H.; Rabinovich, Y. I. Hydrophobic interactions between dissimilar surfaces. *J. Colloid Interface Sci.* **1997**, *185* (2), 363−370.
(63) Bar, G.; Thomann, Y.; Brandsch, R.; Cantow, H.-J.; Whangbo, M.-H. Factors affecting the height and phase images in tapping mode atomic force microscopy. Study of phase-separated polymer blends of poly (ethene-co-styrene) and poly (2, 6-dimethyl-1, 4-phenylene oxide). *Langmuir* **1997**, *13* (14), 3807−3812.
(64) Yan, Y.; Huang, J.; Tang, B. Z. Kinetic trapping−a strategy for directing the self-assembly of unique functional nanostructures. *Chem. Commun.* **2016**, *52* (80), 11870−11884.

https://doi.org/10.1021/acs.nanolett.2c00332
Nano Lett. 2022, 22, 5077−5085